

Analysis for mechanical characteristics and failure models of coal specimens with non-penetrating single crack

Huayong Lv^{1,2,3a}, Yuesong Tang^{1,3}, Lingfei Zhang^{1,3}, Zhanbo Cheng^{*1,3,4} and Yanning Zhang^{1,3}

¹School of Resource and Safety Engineering, China University of Mining and Technology (Beijing), Beijing 100083, China

²State Key Laboratory of Coal Resources and Safe Mining, China University of Mining and Technology, Xuzhou 221116, China

³Coal Industry Engineering Research Center of Top-coal Caving Mining, Beijing 100083, China

⁴School of Engineering, University of Warwick, Coventry CV47AL, U.K.

(Received January 7, 2019, Revised February 20, 2019, Accepted February 24, 2019)

Abstract. It is normal to observe the presence of numerous cracks in coal body. And it has significantly effective on the mechanical characteristics and realistic failure models of coal mass. Therefore, this paper is to investigate the influence of crack parameters on coal body by comprehensive using theoretical analysis, laboratory experiments and numerical simulation through prepared briquette specimens. Different from intact coal body possessing single peak in stress-strain curve, other specimens with crack angle can be illustrated to own double peaks. Moreover, the unconfined compressive strength (UCS) of specimens decreases and follow by increasing with the increase of crack angle. It seems to like a parabolic shape with an upward opening. And it can be demonstrated that the minimum UCS is obtained in crack angle 45°. In terms of failure types, it is interesting to note that there is a changing trend from tensile failure to tensile-shear mixing failure with tension dominant follow by shear dominant with the increase of crack angle. However, the changing characteristics of UCS and failure forms can be explained by elastic-plastic and fracture mechanics. Lastly, the results of numerical simulations are good consistent with the experimental results. It provides experimental and theoretical foundations to reveal fracture mechanism of coal body with non-penetrating single crack further.

Keywords: unconfined compressive strength; non-penetrating single crack; crack angle; failure form

1. Introduction

It is fact that numerous cracks are formed in various geotechnical materials, such as coal and rock body. Obviously, the mechanical behaviours and failure forms of materials as well as the geometry of fractures depend largely on the distribution and evolution of cracks (Bagheripour *et al.* 2011, Erarslan 2016, Komurlu *et al.* 2016, Shen and Barton 2018, Zhou *et al.* 2015, Panaghi *et al.* 2015, Sun *et al.* 2018, 2017). This process can be observed in many conditions, such as top-coal caving face, rip spalling. Therefore, this problem has been attracted great attention, especially for coal seam with cracks occurring.

Obviously, the confining pressure was key factor to depend on the failure mode of specimens under triaxial compression (Mohammadi and Tavakoli 2015). However, in terms of uniaxial compressive test, the strength and failure mode with cracks were closely related to crack angle, width, spacing and number as well as loading rate. Especially for the length of rock bridge smaller than crack length, failure mode of rock samples was caused by the joint action of single and multiple fractures (Yang *et al.* 2013). Meanwhile, various numerical simulation methods

were also used to reveal the failure process and ultimate failure mode, crack propagation, mechanical properties of rock specimens under the effect of various crack physical parameters (Fu *et al.* 2017, Yang *et al.* 2013, Gonçalves da Silva and Einstein 2013, Wang *et al.* 2014, Zhao *et al.* 2015, Cao *et al.* 2017). Especially, CT scanner technology was also employed to identify the position and propagation of inside crack in specimens (Lu *et al.* 2015). Moreover, the method of field measurement was adopted to investigate the distribution and development of structure cracks in coal seams by Song (1998). Especially for top-coal caving workface, there are a large number of tiny joint cracks in top coal as well as tensile stress would be formed with the action of continuously dynamic stress. And the crack continued to spread until top coal failure or cut (Zhang and Wu 2000). Therefore, the number of crack groups, azimuth, spacing and their matching with working face position are the key factors that affects the caving ability of coal seam. And shear failure was dominant in top-coal caving workface according to the crack development and failure degree of top-coal (Wang and Yang 2009, Wang 2018). Moreover, the failure range of coal wall can also be obtained based on the evolution of cracks in coal seam (Liu *et al.* 2008, Yang *et al.* 2013). In terms of theoretical foundations, rock strength obeyed Weibull distribution and the mechanical characteristics, failure process and morphology of rock specimens were also revealed (Tang 1998, 2000a, b).

The existing findings considering the geometry and

*Corresponding author, Ph.D. Student

E-mail: Z.Cheng.4@warwick.ac.uk

^aPh.D. Student

spatial position of cracks focused on single crack, non-parallel/parallel multiple sets of cracks and composite cracks (Haeri *et al.* 2014, 2015, Sarfarazi *et al.* 2017, Zhou *et al.* 2018, Fu *et al.* 2017, Wang and Tian 2018). However, there are few researches focusing on investigating the influence of crack angle on the mechanical parameters and failure forms of coal samples by comprehensive using theoretical analysis, experiment tests and numerical simulation. Therefore, it is necessary to illustrate coal body with non-penetrating single crack in order to deeply explore the failure mechanism top-coal and coal wall. In this paper, comprehensive methods are selected to reveal the mechanical properties and the evolution of failure modes of coal samples with the increase of crack angle.

2. Experimental work

2.1 Sample preparation

In order to study the influence of crack behaviours on the mechanical properties and failure modes of coal body, the pulverized coal is screened by 0.5 mm aperture sieve followed by mixed with cement and proper moisture content. And the specific mass ratio of pulverized coal, cement content and moisture content are 1.5:1.5:1. Moreover, the standard intact and single-crack coal specimens were prepared with diameter 50 mm and height 100mm. For obtaining non-penetrating single crack with different angle (0°, 15°, 30°, 45°, 60°, 75° and 90°) in coal samples, the steel slice was adopted to pre-insert into the moulds. Before performing unconfined compressive tests, all samples were cured with 15 days at a room temperature of 30°C. The details of specimen parameters and partial specimens are listed and shown in Table 1 and Fig. 1, respectively.

2.2 Test apparatus and testing schemes

The TAW2000 micro-computer-controlled electro hydraulic servo universal testing machine was used in this study as shown in Fig. 2. It is mainly composed of the following parts: 600kN axial actuator, axial load and displacement transducers, screen display and testing results treatment. The device can be regarded as a rigid test machine because the failure strengths of both the coal and rock are very small in relation to the measurement range of the test apparatus. Therefore, it meets the requirement of the International Society for Rock Mechanics (Hatheway 2009). The uniaxial compressive tests were performed with strain-controlled and the loading rate was 0.5 mm/min. During the process of loading, high-speed camera was used to record the whole failure process of specimens from crack initiation to propagation until complete destroyed.

2.3 Results and discussion

2.3.1 Whole stress-strain curve

Uniaxial compressive tests were performed for specimens with intact and different crack angles. Meanwhile, the number of specimens with same condition are four and the average results of each series are adopted to

Table 1 Details of specimen parameters

Specimen parameters	Angle/°	Number of specimens	Length/mm
Crack specimen	0/15/30/45/60/75/90	28	40
Intact specimen	-	4	-



Fig. 1 Partial samples



Fig. 2 Experimental equipment

insure its reliable and accurate. The corresponding details of whole stress-strain curves are illustrated in Figs. 3 and 4.

It can be observed that the whole stress-strain curve underwent five stages: compaction stage, linear elastic deformation stage, inelastic deformation stage, strain-hardening stage, post-peak softening stage. The initial compaction stage showing an inelastic was concave-upward shape because of the closure of the existing microcracks. This was followed by linear elastic deformation stage. The slope of straight line can be regards as the average elastic modulus of coal specimens because the material exhibited intact geomaterial behaviour with a constant stiffness during this stage. With the continuous increase in the stress, the specimens entered a inelastic deformation stage, during which the non-linearity can be demonstrated because there was a significant increase in the strain occurred as the cracks gradually form and propagate in a stable manner. And the specimens reached the initial yield point when the axial stress was up to roughly 80% of peak strength. The subsequent strain hardening stage dominated a strain increase in an unstable manner up to the peak stress of 7.8 MPa as well as an asymptotic failure state was observed. After peak stress point, there was a post-peak softening stage characterised by the crack inside specimens beginning to unsteady propagate and fulling of all material. And it caused the internal structure highly disrupted. Therefore, the stress exhibited brittle drop with the continuous increase of strain.

It can be observed that the whole stress-strain curve underwent five stages: compaction stage, linear elastic deformation stage, inelastic deformation stage, strain-hardening stage, post-peak softening stage. The initial compaction stage showing an inelastic was concave-upward shape because of the closure of the existing microcracks. This was followed by linear elastic deformation stage. The

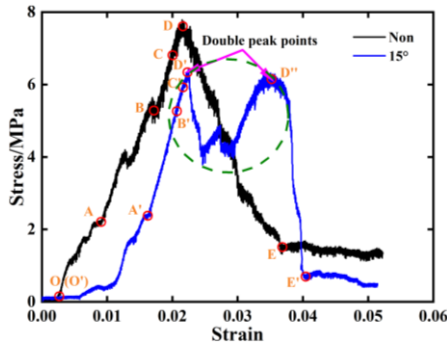


Fig. 3 Comparison of stress-strain curves for intact and cracked specimens

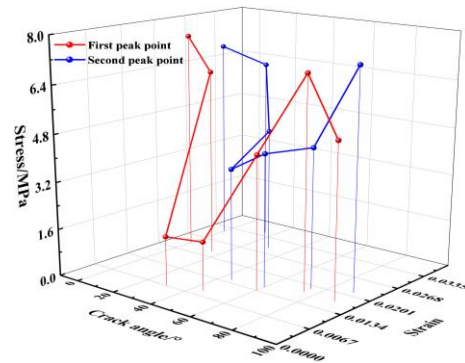


Fig. 5 UCS in different peak points

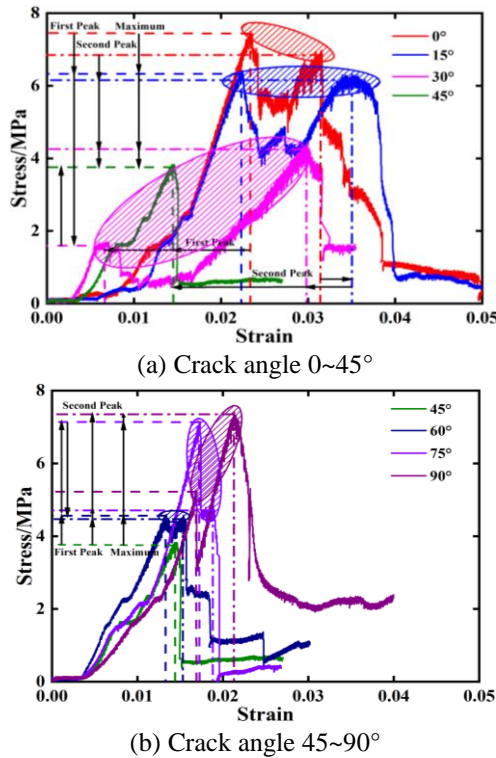


Fig. 4 Whole stress-strain curve

slope of straight line can be regarded as the average elastic modulus of coal specimens because the material exhibited intact geomaterial behaviour with a constant stiffness during this stage. With the continuous increase in the stress, the specimens entered an inelastic deformation stage, during which the non-linearity can be demonstrated because there was a significant increase in the strain occurred as the cracks gradually form and propagate in a stable manner. And the specimens reached the initial yield point when the axial stress was up to roughly 80% of peak strength. The subsequent strain hardening stage dominated a strain increase in an unstable manner up to the peak stress of 7.8MPa as well as an asymptotic failure state was observed. After peak stress point, there was a post-peak softening stage characterised by the crack inside specimens beginning to unsteady propagate and fulling of all material. And it caused the internal structure highly disrupted. Therefore, the stress exhibited brittle drop with the continuous increase of strain.

In terms of specimens with non-penetrating single crack, there were five stages as well for the whole stress-strain curve. However, the initial compaction stage was more obvious. Although the change of elastic modulus can be ignored, the value of crack angle contributed on the range of strain in linear elastic deformation stage. To be specific, this range decreased followed by increasing with the increase of crack angle. Moreover, the obviously characteristic in specimens with different crack angle was that a double peak points can be observed compared with the whole stress-strain of intact specimen. It can be explained that the cracks would rapidly propagate to cut the specimens into blocks along with emitting an obvious failure noise at the first peak point causing the loading capacity of material dropped significantly. On the other hand, with the continuous increase of strain, the crushed coal blocks were compacted again until reaching the second peak value.

2.3.2 Variation of mechanical parameters with crack angle

Fig. 5 demonstrates the change trend of UCS in first and second peak points with different crack angles. It is observed that three categories can be divided in terms of the specific strain values occurring first peak point according to the crack angle. The maximum compressive stress is obtained with 6~7 MPa when the strain is around 0.025 for the crack angle of 0° and 15°. And the maximum compressive stress reduces to about 1.6MPa for the crack angle of 30° and 45° under the strain of roughly 0.01. However, if the crack angle increases to more than 60°, the maximum compressive stress raises again to the range of 4~7MPa occurred with the strain of approximately 0.015.

However, the conditions of second peak point are rather more complex. To be specific, the second peak point occurs when the strain is about 0.03 for the crack angles of 0°~30°, while the strain under same condition decreases to around 0.015 for the crack angles of 45° and 60° followed by arising to approximately 0.02 again for the crack angles of 75° and 90°. In terms of maximum compressive stress in second stage, expect for the crack angle of 0°, 15° and 90° with the maximum compressive stress more than 6.2MPa, this value can be revealed in the range of 3.7~4.7 MPa for other conditions. It is interesting to note that the strain occurring first peak point is usually in the range of 0.01 to 0.025, while this value has an increment of 0.005 in the

Table 2 The relative parameters of fitting curves

Polynomial order	Intercept	x	x^2	x^3	x^4	x^5	x^6	R^2
2	7.7048	-0.1529	0.0017	-	-	-	-	0.8439
3	7.8548	-0.1862	0.0027	-7.4074×10^{-4}	-	-	-	0.8529
4	7.5022	0.0450	-0.0108	2.3636×10^{-4}	-1.3543×10^{-6}	-	-	0.9943
5	7.5093	0.0258	-0.0090	1.7834×10^{-4}	-6.1354×10^{-7}	-3.2922×10^{-9}	-	0.9947
6	7.5000	0.2417	-0.0378	0.0015	-2.9355×10^{-5}	2.7984×10^{-7}	-1.0486×10^{-9}	1.0000

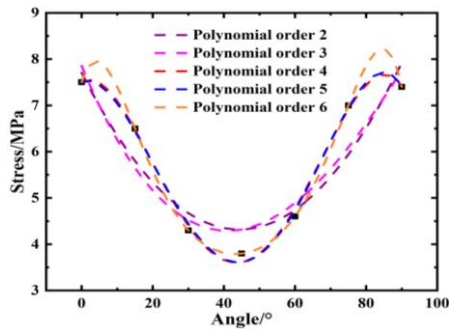


Fig. 6 UCS under different inclinations

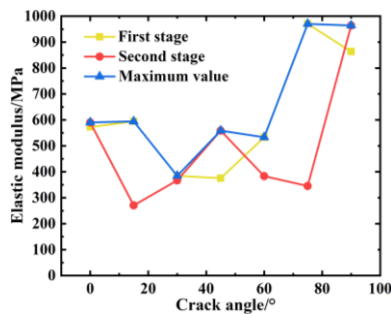


Fig. 7 Elastic modulus in different stages

second peak point. For both peak points, the strain usually decreases followed by increasing with the increase of crack angle.

Selecting the maximum compressive stress as the ultimate UCS, the value can be shown in Fig. 6 with the increase of crack angle.

Obviously, UCS decreases followed by increasing with the increase in crack angle. And the variation trend is basically “V” shape with axial symmetry in position of crack angle equalling to 45° , which is consistent with the strength theory of single structure plane proposed by Jaeger and Cook (1981). It means the minimum UCS of coal specimens with non-penetrating single crack is obtained when the crack angle is 45° . And there is marginal difference of UCS in terms of both conditions of crack angle with 0° and 90° . They are 7.8MPa and 7.4MPa, respectively. Therefore, the inclination angle of cracks in coal mass has significant influence on its strength.

Moreover, polynomial type empirical formula is adopted to fit UCS versus crack angle as shown in Fig. 6. The relative coefficients of various orders can be listed in Table 3. It can be observed the multiple correlation coefficient square (R^2) increases with the increase of polynomial order. On the other hand, the larger polynomial order can cause computing process difficulty and complexity in practice.

Therefore, selecting polynomial order as 4 can be regarded as the most reasonable value for balancing accuracy and practicability. And the corresponding equation to present the relationship of UCS versus crack angle can be obtained from Table 2.

On the other hand, compared with the elastic modulus in different crack angles, the minimum value can be observed with the crack angle of 45° in first stage, while the crack angle of 30° in second stage occurs the minimum elastic modulus as shown in Fig. 7. Combined with two stages, the maximum elastic modulus will be revealed in the crack angle more than 75° , and 30° obtains the minimum elastic modulus. However, other conditions have similar elastic modulus.

2.3.3 Crack propagation process and failure mode

The inclination angle of pre-existing crack plays the key role in the propagation process of cracks and contributes on the ultimate failure mode and UCS of specimens. It is necessary to illustrate the propagation mechanism of crack in coal specimens with different crack angle under uniaxial compressive. The genuine evaluation process and corresponding sketch up of ultimate failure modes can be revealed in Fig. 8.

In terms of intact specimen, there was almost no crack appeared along with the material compacted slowly at the initial stage of axial loading. However, the fracture can be formed in the upper end of sample with the increase of strain. And it can be presented that the subsequent propagation direction of crack was parallel to the direction of the maximum principle stress. The increase of fractures number and length was followed until various macroscopic main crack influencing the stability of specimen appeared in the middle and two sides of specimen. Finally, the coal mass was cut as long strip along with coal flaked in the surface. And tensile failure can be expressed as the ultimate failure mode of intact specimen.

On the other hand, although the initial process of specimens with the presence of crack was basically similar to that of intact specimen, such as the coal flaking appearing on the surface as well, the failure mode has significant different. Two failure modes with shear failure in crack surface and tensile failure along the vertical direction of crack surface can be represented with the continuous increase of crack angle in coal specimens. To be specific, the direction of pre-existing crack can be regarded as perpendicular to the direction of the maximum principle stress under both condition of α equalling to 0° and 15° . Therefore, the main macroscopic cracks were formed in the vertical direction of crack surface as shown in Figs. 8(b)-

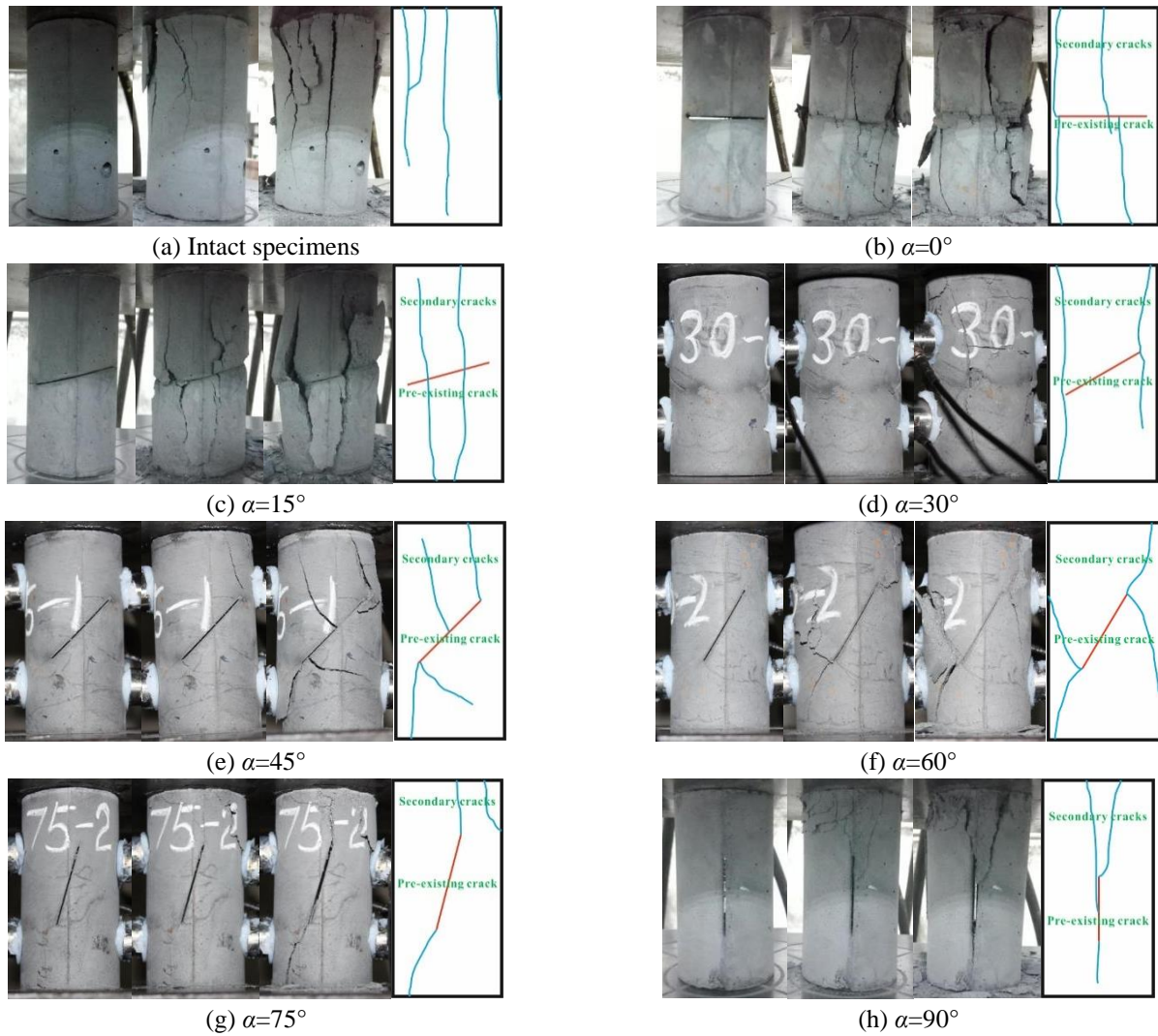


Fig.8 Crack propagation process and ultimate failure mode

8(c), respectively. The failure mode under these conditions can also be regarded as main tensile failure. However, with the continuous increase of crack angle reaching to 30°, 45°, 60° and 75°, respectively, there was an obvious angle occurring between crack surface and loading direction. It caused the crack surface and the coal bodies on both sides to be subjected to both shear and compression simultaneously. In detail, partial shear failure appeared at the two ends of the crack, leading to secondary fracture formed with a wing type with a crack angle of 30° and 45°. The results were that the main failure of specimens exhibited in the middle position under the influence of various macroscopic cracks as shown in Figs. 8(d)-(e), respectively. The failure modes can be expressed as tensile-shear mixed failure with tension dominant. However, there was coal mass falling directly along the crack surface in the process of uniaxial compression when the crack angles were 60° and 75°. And one or two main secondary fractures can be observed through the pre-existing crack near its tip with a wing form as well. Tensile-shear mixed failure with shear dominant was the failure mode under both conditions as shown in Figs. 8(f) and 8(g), respectively. Finally, it is interesting to note that the failure mode of specimens with a crack angle of 90° was

similar to intact specimens again due to the axial loading mainly acting on coal blocks with the pre-existing crack beginning at its tips as shown in Fig. 8(h).

3. Mechanical analysis of coal mass with single crack

3.1 Weak plane effect of prefabricated crack strength

As shown in Fig. 9, the angle of a single crack (AB) and the minimum principal stress (σ_3) can be expressed as α . And the normal stress (σ) and shear stress (τ) acting on the crack surface are given as follows (Liu *et al.* 2014).

$$\begin{cases} \sigma = \frac{1}{2}(\sigma_1 + \sigma_3) + \frac{1}{2}(\sigma_1 - \sigma_3)\cos 2\alpha \\ \tau = \frac{1}{2}(\sigma_1 - \sigma_3)\sin 2\alpha \end{cases} \quad (1)$$

where σ_1 is the maximum principal stress.

In terms of uniaxial compressive test, there is unconfined pressure with σ_3 equaling to zero. And the Eq. (1) can be simplified as follows

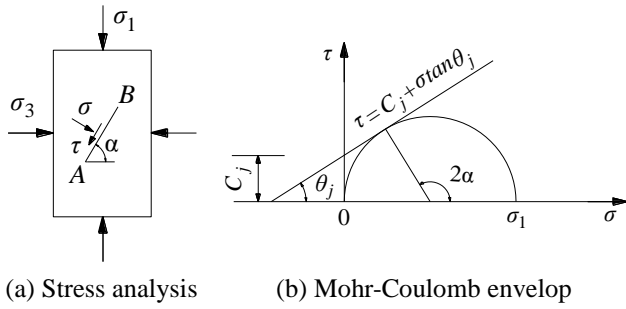


Fig. 9 Theoretical analysis of surface strength with single crack structural

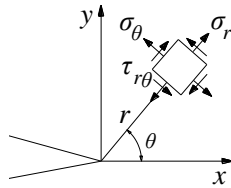


Fig. 10 Extreme component of stress at crack tip

$$\begin{cases} \sigma = \frac{1}{2} \sigma_1 (1 + \cos 2\alpha) \\ \tau = \frac{1}{2} \sigma_1 \sin 2\alpha \end{cases} \quad (2)$$

According to Mohr-Coulomb criterion, Eq. (3) can express the failure condition of specimen along the crack plane.

$$\tau = C_j + \sigma \tan \theta_j \quad (3)$$

where C_j and θ_j are the cohesive and internal friction angle of coal mass with single crack structural.

Therefore, combined with Eqs. (2)-(3), the critical maximum principle stress causing coal mass failure can be expressed as follows

$$\sigma_1 = \frac{2C_j}{(1 - \tan \theta_j \cot \alpha) \sin 2\alpha} \quad (4)$$

It should be noted the critical maximum principle stress tends to infinite if the crack angles are 0° and 90° or equal to internal friction angle. In fact, it is impossible for σ_1 keeping increase without specimen failure. Therefore, it is reasonable to express that the specimen will be failure in a certain direction rather than along the crack surface under these conditions. On the other hand, the relationship of crack angle and internal friction angle of coal mass can be presented as follow when the specimen slips along crack plane.

$$\alpha = \frac{\pi}{4} + \frac{\theta_j}{2} \quad (5)$$

It should be noted that the experimental results in this paper is consistent with the results of shear experiments performed by Wang (2017). It shown that the angle of main

single crack with the minimum principle stress (α) was 62.5° when the internal friction angle of coal mass (θ_j) was 35°

3.2 Stress-strain field and fracture criterion at crack tip

Based on the maximum axial tensile stress criterion without considering closure effective as well, the stress-strain field in the zone of crack tip is shown in Fig. 10 and it can be expressed with polar coordinate as follow (Li *et al.* 2005).

$$\sigma_r = \frac{1}{2\sqrt{2\pi r}} \left[K_{\text{I}} (3 - \cos \theta) \cos \frac{\theta}{2} + K_{\text{II}} (3 \cos \theta - 1) \sin \frac{\theta}{2} \right] \quad (6)$$

$$\sigma_\theta = \frac{1}{2\sqrt{2\pi r}} \cos \frac{\theta}{2} \left[K_{\text{I}} (1 + \cos \theta) - 3K_{\text{II}} \sin \theta \right] \quad (7)$$

$$\tau_{r\theta} = \frac{1}{2\sqrt{2\pi r}} \cos \frac{\theta}{2} \left[K_{\text{I}} \sin \theta + K_{\text{II}} (3 \cos \theta - 1) \right] \quad (8)$$

$$\varepsilon_\theta = \frac{1}{2E\sqrt{2\pi r}} \left[K_{\text{I}} \cos \frac{\theta}{2} (1 - 3\nu + \cos \theta + \nu \cos \theta) - K_{\text{II}} (3 \cos \frac{\theta}{2} \sin \theta + 3\nu \sin \frac{\theta}{2} \cos \theta - \nu \sin \frac{\theta}{2}) \right] \quad (9)$$

where σ_r , σ_θ , $\tau_{r\theta}$ and ε_θ are the radial stress, tangential stress, shear stress and strain of a point around single crack, respectively. E and ν are the elastic modulus and Poisson's ratio of coal mass, respectively. r is the distance from the tip of single crack to a point around crack. θ is the angle between a straight line connecting crack tip with a point around crack and horizontal direction. K_{I} and K_{II} are the stress intensity factor at the inner tip of crack.

Each crack tip has different under uniaxial compressive process. The stress-strain field in the zone of crack tip can be resolved through Eqs. (6)-(9). when stress intensity factor can be accurate obtained. And it means K_{I} is less than zero if the crack is not closed (Gou and Sun 2002). Erdogan and Sih (1963) firstly proposed the criterion of maximum circumferential tensile stress. Assuming that the crack propagates along the direction of maximum circumferential stress under compressive loading, the cracks begin to develop and propagate when $\sigma_{\theta\text{max}}$ equals to $\sigma_{\theta\text{c}}$. And the criterion of crack beginning to propagate can be illustrated as follows

$$\cos \frac{\theta_0}{2} \left[K_{\text{I}} \cos^2 \frac{\theta_0}{2} - \frac{3}{2} K_{\text{II}} \sin \theta_0 \right] = K_{\text{Ic}} \quad (10)$$

where K_{Ic} and θ_0 are fracture toughness and crack angle, respectively.

3.3 Crack propagation model

Under uniaxial compression conditions, the crack propagation mode in coal specimen can be summarised with six types as shown in Fig. 11 (Cen and Huang 2014).

Model I: wing crack and stretching. These cracks have the same formation mechanism and propagate path along

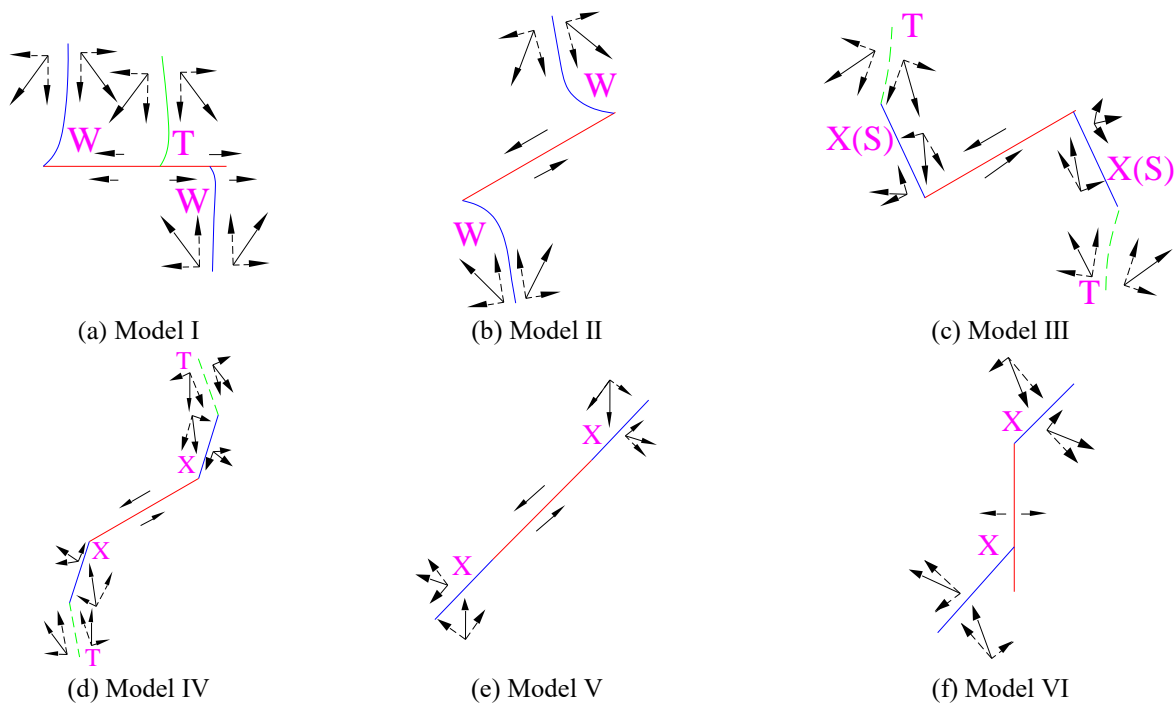


Fig. 11 Basic modes of coal mass with crack expansion, T-Pull crack;W-Wing crack, S-shear crack and X-Composite crack

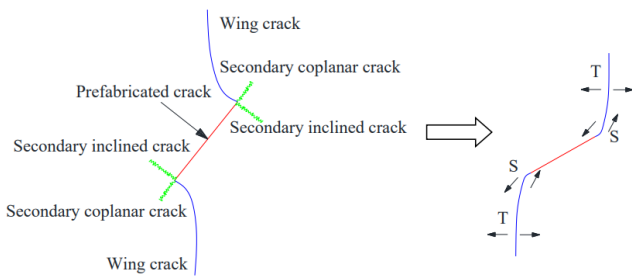


Fig. 12 Typical propagation modes of coal mass with single crack

the direction of maximum principal stress, while the initial development position is different. It can be usually observed under the condition of α as 0° .

Model II: consistent with wing crack. In this model, the initial developing position is at the crack tip and the crack propagates along the direction of the maximum principal stress. The crack angles in the range from 15° to 60° normally possesses these phenomena.

Mode III: anti-wing composite crack and stretching. This pattern often occurs in crack angle with 0° , 15° , 30° , 60° and 75° . The characteristics of this model is that an anti-wing crack or shear crack is formed at the tip of single crack (solid line segment). And the direction of crack evolution towards to the direction of the maximum principle stress (dashed line segment).

Mode IV: consistent with wing composite crack and stretching. It is similar to the former in the occurrence conditions of crack angle. However, it often appears at one or both ends of single crack.

Mode V: coplanar composite crack. The crack propagates from the tip of the crack with the opposite this model. It can be found at the crack angle of 45° .

Mode VI: inclined composite crack. It should be noted this model only can be demonstrated with crack angle 90° . Crack extends upward or diagonally downward occurring at the either side of crack or its tip.

The common propagation modes of coal mass with non-penetrating single crack under uniaxial compression are revealed in Fig. 12 (Sagong and Bobet 2002), which is consistent with the analysis in Fig. 11. However, two types of secondary cracks caused by shearing mechanism are generally considered. Among of them, S and T refer to shear cracks and tensile cracks, respectively.

4. Numerical simulation

4.1 Model establishment

RFPA system (Rock Failure Process Analysis System) was adopted to describe the evolution process of single crack in coal mass. It bases on elastic mechanics as stress analysis tool as well as elastic damage theory and modified Coulomb failure criterion are considered as the principle of medium deformation and failure analysis modules.

The length and width of specimen are 100 mm and 50 mm, respectively. And the pre-existing crack is set up with the length of 40 mm and the width of 1 mm. Meanwhile, the whole model grid is divided into 20000 elements. In terms of crack angle, it is consistent with experiment conditions as well. The relative micro-mechanical parameters of model are calculated from the macro-mechanical parameters of experiment results as shown in Table 3. The Micro-mechanical parameters and Macro-mechanical parameters of the rock mass can be linked through the mean coefficient. The expressions can be shown as follows

$$f/f_0=0.2602\ln m+0.0233 \quad (1.2 < m < 50) \quad (11)$$

$$E/E_0=0.1412\ln m+0.6476 \quad (1.2 < m < 10) \quad (12)$$

where f and f_0 are macro-compressive strength and micro-compressive strength, respectively. E and E_0 are macro-elastic modulus and micro-elastic modulus, respectively. m is homogeneous degree, it was selected as 2 in this manuscript because this value can better represent the properties of coal mass (Tang, 1998).

Moreover, Fig. 13 illustrates the basic numerical model of coal specimen with non-penetrating single crack. In all specimens, Mohr-Coulomb criterion and plane stress model are selected and the increment is 0.01 mm each step controlled by displacement loading mode because the stress-strain curves under this condition are consistent with the results of lab tests.

4.2 Results and discussions

4.2.1 Stress-strain curve

As shown in Fig. 14, the whole stress-strain curve of intact specimen obtained from the numerical simulation is similar to the experimental results. It can also be divided into five stages. And the peak stress and residual stress are 8.3 MPa and 1.1 MPa, respectively, which are better match the experiment results. Therefore, it is a reliable method for using RFPA system to explore the characteristics of coal mass with single crack.

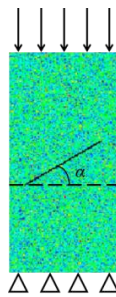


Fig. 13 Numerical model

Table 3 Micro-mechanical parameters of specimen

Homogeneous degree	Mean elastic modulus/MPa	Mean compressive strength/MPa	Poisson ratio	Angle of friction / °	Pressure rabbi
2	1333	39	0.3	35	15

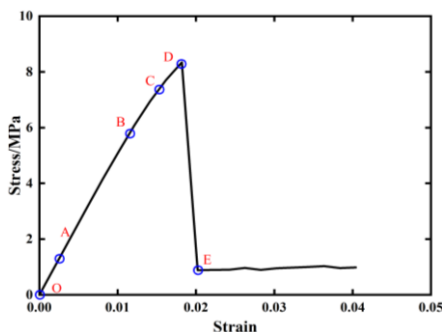


Fig. 14 Stress-strain curve of intact specimen

4.2.2 Shear stress evolution process

Obviously, the equilibrium state of internal stress is interrupted leading to its redistribution. And the local stress concentration is firstly formed around the single crack as shown in Fig. 15. Moreover, the evolution process of single crack depends on its angle.

In terms of intact specimen, it takes place in original stress state without obvious changing in the initial loading stage. However, as the continuous loading, there is internal damage appeared and stress redistribution observed. It causes the local stress concentration around damage zone followed by the specimen completely failure with main macroscopic cracks occurred as shown in Fig. 15(a). On the other hand, the high stress concentration at both ends of pre-existing single crack can be always revealed in all loading process. At the initial loading stage, the local stress concentration only appears around the zone of prefabricated crack followed by causing coal mass failure around this area and secondary fracture formed. Therefore, the local stress concentration continues to occur at the cracks tip and expand the main and secondary fractures until the specimen complete destroyed with the continuous preform of loading process as shown in Figs. 15(b)-15(h).

4.2.3 Failure mode and internal energy accumulation of specimen

The failure modes of specimens obtained from numerical simulation are illustrated as shown in Fig. 16. There are various main macroscopic cracks and micro cracks occurring in intact specimen. And the propagation direction of main cracks is parallel to the direction of maximum principle stress. It can be regards as typical brittle fracture failure or tensile failure as shown in Fig. 16(a).

According to the Figs. 16(b) and 16(c), the wing cracks are formed at the both ends of pre-existing crack as well as the tensile crack through crack surface can also be observed followed by expending along with the direction of maximum principle stress until the specimen completely failure due to axial spitting failure surface. And this mode can be boiled down to tensile failure.

However, expect for wing crack, the secondary fractures are also formed at both ends of pre-existing crack and usually propagate along the direction of maximum principle stress as well with the crack angle of 30° and 45°. Obviously, the secondary fractures have significant influence on ultimate failure surface. There are axial splitting failure surface and inclined shear plane along the pre-existing crack in specimens. This mode can be called.

With the increase of single crack angle, the mode transfers to tensile-shear mixing failure with shear dominant. Although there are also secondary fractures formed at the both ends of pre-existing cracks, they have marginal effect on the formation of failure surface with the crack angle of 60° and 75°. And the crack can develop through all specimen in axial direction with the crack angle of 90°. It finally forms the typical axial splitting failure mode causing by tensile stress. In a word, all results in numerical simulation are better consistent with the corresponding results of laboratory experiments.

Taking the crack angle of 15° as example, the internal energy variation of specimens is analysed and described

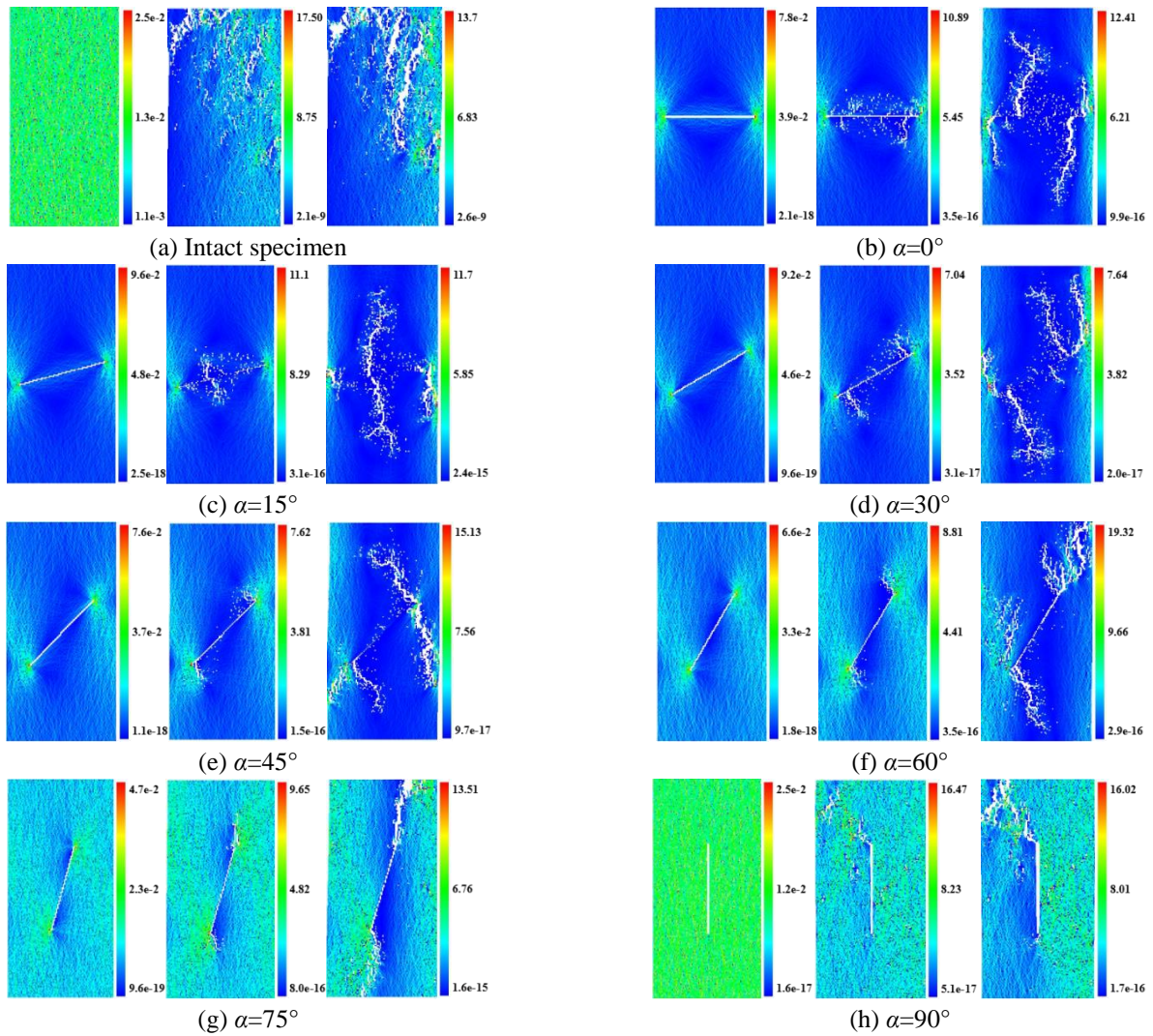


Fig. 15 Evolution of shear stress (MPa)

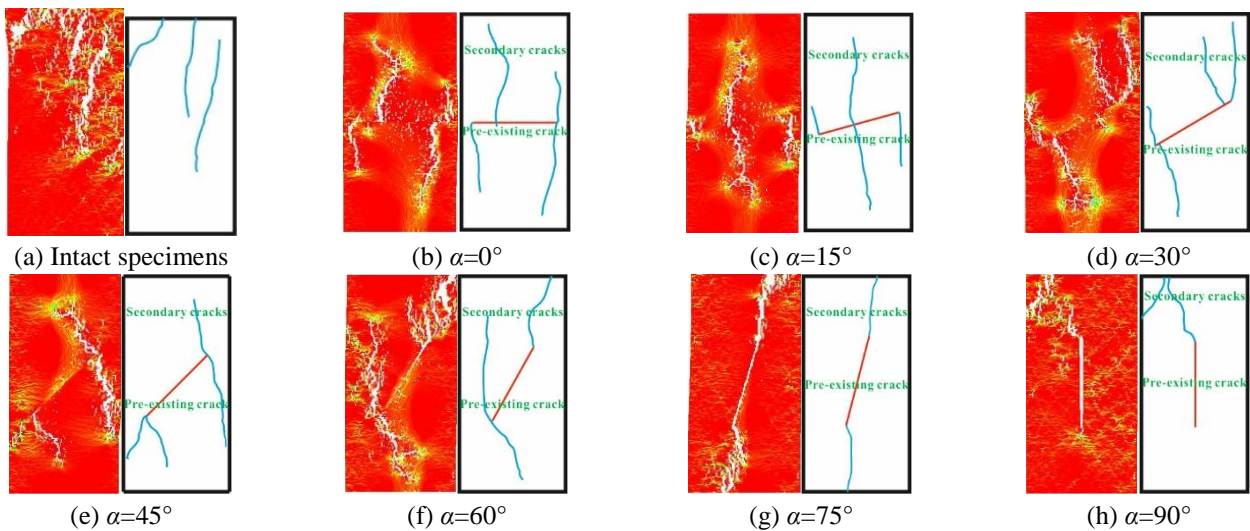


Fig.16 Ultimate failure mode

in Fig. 17. At the initial loading stage, the number of acoustic emissions is small indicating the deformation of material slowly. However, the acoustic emissions increase sharply reaching the two peak points of A and B with the

continuous loading. It also means the deformation of material increasing as well. Moreover, the accumulate number of acoustic emissions after point C has marginal increment and trends to keep steady. It indicates that the

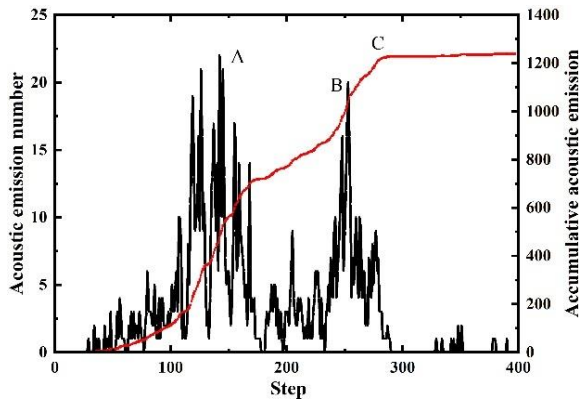


Fig. 17 Acoustic emission in specimen ($\alpha=15^\circ$)

specimen completely damages. It should be noted that the internal energy variation of specimens with different crack angle is similar to the currently condition.

5. Conclusions

This paper presents the mechanical characteristics and failure models of coal specimens with non-penetrating single crack combined with comprehensive methods, such as laboratory experiments, theory analysis and numerical simulation. The following conclusions may be drawn from the current study.

- Expect for intact specimen and the crack angle of 90° , it can be observed that there are doubled peak points in whole stress-strain curve. And with the increase of crack angle, the range of strain in linear elastic deformation stage decreases followed by increasing, while the change of elastic modulus can be ignored. And the variation trend of specimen UCS exhibits “V” shape with axial symmetry in position of crack angle equaling to 45° . It means the minimum UCS of coal specimens with non-penetrating single crack is obtained with the crack angle of 45° .

- The failure criterion of specimen along crack surface is achieved by adopting elastic-plastic mechanics and fracture mechanics. According to the criterion of maximum axial tensile stress, the stress-strain field in the zone of crack tip and crack evolution criterion are obtained. Six basic propagation models of crack in coal mass are illustrated.

- With the increase of crack angle, the failure mode is tensile failure (intact specimen, 0° and 15°) followed by tensile-shear mixing failure with tension dominant (30° and 45°) transferred to tensile-shear mixing failure with shear dominant (60° and 75°) and changed to tensile failure again (90°).

Acknowledgements

The first author wishes to acknowledge the financial support from State Key Laboratory of Coal Resource and Safety Mining, China University of Mining and Technology (SKLCRSM18KF023). The corresponding author wishes to acknowledge the financial support from China Scholarship Council (CSC). The authors would also like to thank the editors and anonymous reviewers for their valuable time and suggestions.

References

- Bagheripour, M., Rahgozar, R. and Pashnesaz, H. (2011), “A complement to Hoek-Brown failure criterion for strength prediction in anisotropic rock”, *Geomech. Eng.*, **3**(1), 61-81.
- Cao, R., Cao, P. and Lin, H. (2017), “Experimental and numerical study of the failure process and energy mechanisms of rock-like materials containing cross un-persistent joints under uniaxial compression”, *Plos One*, **12**(12), e0188646.
- Cen, D.F. and Huang, D. (2014), “Mesoscopic displacement modes of crack propagation of rock mass under uniaxial compression with high strain rate”, *J. China Coal Soc.*, **39**(3), 436-444.
- Erarslan, N. (2016), “Microstructural investigation of subcritical crack propagation and fracture process zone (FPZ) by the reduction of rock fracture toughness under cyclic loading”, *Eng. Geol.*, **208**, 181-190.
- Erdogan, F. and Sih, G.C.J. (1963), “On crack extension in plates under plane loading and transverse shear”, *J. Basic Eng.*, **85**(4), 519-527.
- Fu, J., Zhang, X. and Zhu, W. (2017), “Simulating progressive failure in brittle jointed rock masses using a modified elastic-brittle model and the application”, *Eng. Fract. Mech.*, **178**, 212-230.
- Gonçalves da Silva, B. and Einstein, H.H. (2013), “Modelling of crack initiation, propagation and coalescence in rocks”, *Int. J. Fracture*, **182**(2), 167-186.
- Gou, S.H. and Sun, Z.Q. (2002), “Closing law and stress intensity factor of elliptical crack under compressive loading”, *Trans. Nonferr. Metal. Soc.*, **5**(12), 966-969.
- Haeri, H., Khaloo, A. and Marji, M.F. (2015), “Experimental and numerical simulation of the microcrack coalescence mechanism in rock-like materials”, *Strength Mater.*, **47**(5), 740-754.
- Haeri, H., Shahriar, K. and Marji, M.F. (2014), “Experimental and numerical study of crack propagation and coalescence in pre-cracked rock-like disks”, *Int. J. Rock. Mech. Min. Sci.*, **67**, 20-28.
- Hatheway, H.W. (2009), “The complete ISRM suggested methods for rock characterization, testing and monitoring, 1974-2006”, *Environ. Eng. Geosci.*, **15**(1), 47-48.
- Jaeger, J.C. and Cook, N.G. (1981), *Rock Mechanics Foundation*, Science Press, Beijing, China.
- Komurlu, E., Kesimal, A. and Demir, S. (2016), “Experimental and numerical analyses on determination of indirect (splitting) tensile strength of cemented paste backfill materials under different loading apparatus”, *Geomech. Eng.*, **10**(6), 775-791.
- Li L.Y., Xu, F.G., Gao, F., Wang, L. and Che, F.X. (2005), “Fracture mechanics analysis of rock bridge failure mechanism”, *Chin. J. Rock Mech. Eng.*, **24**(23), 4328-4334.
- Liu, C.Y., Huang, B.X., Chang, X.M., Wang, J. and Wei, M.T. (2008), “Study on tip to face coal and rock stability control of fully mechanized stepped large cutting height mining in extremely soft thick seam”, *J. China U. Min. Technol.*, **37**(6), 734-739.
- Liu, J.J. and Chen, L.Y. (2014), “Numerical analysis on strength characteristics of sandstone samples failure with single fracture in the condition of uniaxial compression”, *Sci. Technol. Eng.*, **14**(25), 282-287, 292.
- Lu, Y., Wang, L. and Elsworth, D. (2015), “Uniaxial strength and failure in sandstone containing a pre-existing 3-D surface flaw”, *Int. J. Fracture*, **194**(1), 59-79.
- Mohammadi, M. and Tavakoli, H. (2015), “Comparing the generalized Hoek-Brown and Mohr-Coulomb failure criteria for stress analysis on the rocks failure plane”, *Geomech. Eng.*, **9**(1), 115-124.
- Panaghi, K., Golshani, A. and Takemura, T. (2015), “Rock failure assessment based on crack density and anisotropy index

- variations during triaxial loading tests”, *Geomech. Eng.*, **9**(6), 793-813.
- Sagong, M. and Bobet, A. (2002), “Coalescence of multiple flaws in a rock-model material in uniaxial compression”, *Int. J. Rock Mech. Min. Sci.*, **39**(2), 229-241.
- Sarfarazi, V., Haeri, H., Marji, M.F. and Zhu, Z.M. (2017), “Fracture mechanism of brazilian discs with multiple parallel notches using PFC2D”, *Period. Polytech. Civ. Eng.*, **61**(4), 653-663.
- Shen, B. and Barton, N (2018), “Rock fracturing mechanisms around underground openings”, *Geomech. Eng.*, **16**(1), 35-47.
- Song, X.M. (1998), “Correlation between distribution of cracks and fissures in top coal and size of fragment of mining with sublevel caving”, *J. China Coal Soc.*, **23**(2), 40-44.
- Sun, W., Zhang, S., Guo, W. and Liu W. (2017), “Physical simulation of high-pressure water inrush through the floor of a deep mine”, *Min. Water Environ.*, **36**(4), 542-549.
- Sun, X.Z., Shen, B. and Zhang, B.L. (2018), “Experimental study on propagation behavior of three-dimensional cracks influenced by intermediate principal stress”, *Geomech. Eng.*, **14**(2), 195-202.
- Tang, C.A. (1998), “Numerical simulation of loading inhomogeneous rocks”, *Int. J. Rock Mech. Min. Sci.*, **35**(7), 1001-1007.
- Tang, C.A. (2000), “Numerical studies of the influence of microstructure on rock failure in uniaxial compression-Part I: Effect of heterogeneity”, *Int. J. Rock Mech. Min. Sci.*, **37**(4), 555-569.
- Tang, C.A. (2000), “Numerical studies of the influence of microstructure on rock failure in uniaxial compression-Part II: Constraint, slenderness and size effect”, *Int. J. Rock Mech. Min. Sci.*, **37**(4), 571-583.
- Wang, J.C. (2018), “Engineering practice and theoretical progress of top-coal caving mining technology in China”, *J. China Coal Soc.*, **43**(1), 43-51.
- Wang, J.C. and Yang, S.L. (2009), “Numerical simulation of mining effect on collapse column activated water Conducting mechanism”, *J. Min. Saf. Eng.*, **26**(2), 140-144.
- Wang, S.Y., Sloan, S.W. and Sheng, D.C. (2014), “Numerical study of failure behaviour of pre-cracked rock specimens under conventional triaxial compression”, *Int. J. Solids Struct.*, **51**(5), 1132-1148.
- Wang, X. and Tian, L. (2018), “Mechanical and crack evolution characteristics of coal-rock under different fracture-hole conditions: A numerical study based on particle flow code”, *Environ. Earth Sci.*, **77**(8), 297.
- Wang, Z.H. (2017), “Failure mechanism and cavability evaluation of the top coal in longwall top-coal caving mining”, Ph.D. Dissertation, China University of Mining and Technology (Beijing), Beijing, China.
- Yang, L., Jiang, Y. and Li, S. (2013), “Experimental and numerical research on 3D crack growth in rocklike material subjected to uniaxial tension”, *J. Geotech. Geoenviron. Eng.*, **139**(10), 1781-1788.
- Yang, S.L., Jiang, H. and Cheng, Z.H. (2013), “Mechanism and control Technology of rib spalling in hard coal seam with developed beddings”, *Coal Sci. Technol.*, **41**(12), 27-30.
- Zhang, Y. and Wu, J. (2000), “Crack-movement degree and caving characteristic of top-coal in longwall top-coal caving mining”, *J. China U. Min. Technol.*, **29**(5), 506-509.
- Zhao, X.G., Cai, M. and Wang, J. (2015), “Objective determination of crack initiation stress of brittle rocks under compression using AE measurement”, *Rock Mech. Rock. Eng.*, **48**(6), 2473-2484.
- Zhou, X., Zhang, J. and Wong, L. (2018), “Experimental study on the growth, coalescence and wrapping behaviors of 3D Cross-Embedded flaws under uniaxial compression”, *Rock Mech. Rock. Eng.*, **51**(5), 1379-1400.
- Zhou, X.P., Bi, J. and Qian, Q.H. (2015), “Numerical simulation of crack growth and coalescence in rock-like materials containing multiple pre-existing flaws”, *Rock Mech. Rock. Eng.*, **48**(3), 1097-1114

CC